Structural and Multidisciplinary Optimization (2022) 65:337
https://doi.org/10.1007/s00158-022-03442-3

RESEARCH PAPER

Topology optimization of stationary fluid–structure interaction problems including large displacements via the TOBS-GT method

K. E. S. Silva[1] · R. Sivapuram[2] · S. Ranjbarzadeh[3] · R. S. Gioria[4] · E. C. N. Silva[3] · R. Picelli[1]

Received: 30 November 2021 / Revised: 14 July 2022 / Accepted: 20 October 2022 / Published online: 15 November 2022

Abstract

This paper addresses the topology optimization of fluid–structure interaction (FSI) systems considering large displacements. We consider the steady-state analysis of flexible structures in contact with a fluid flow governed by the incompressible Navier–Stokes equations. The optimization method used in this work considers the physical analysis and optimization module in a decoupled form. The decoupled analysis allows the finite element problem to be meshed and solved accordingly to the physics requirements. Optimized geometry is constructed by reading and trimming out from an optimization grid described by a set of binary $\{0, 1\}$ design variables. The method is so-called TOBS (Topology Optimization of Binary Structures) with geometry trimming (TOBS-GT). Displacements are resolved using an elastic formulation with geometrical nonlinearities to allow for large deformations. The FSI system is solved by using finite elements and the Arbitrary Lagrangian–Eulerian (ALE) method. Low Reynolds numbers are assumed. The sensitivities are calculated using semi-automatic differentiation and interpolated to optimization grid points. In order to consider large displacements, a mapping between material and spatial coordinates is used to identify and track the deformed configuration of the structure. The optimized binary topology is found by using the standard TOBS approach (Sivapuram and Picelli in Finite Elem Anal Des 139:49–61, 2018) based on sequential integer linear programming. Numerical examples show that the TOBS-GT method can be effectively applied to design 2D and 3D structures in FSI problems including nonlinear structural responses.

Keywords Topology optimization · Fluid–structure interaction · Binary design variables · Large displacements

1 Introduction

Fluid–structure interaction (FSI) is a very common multiphysics phenomenon in nature, present in different proportions and areas of application (Casadei et al. 2001; Galdi and Rannacher 2010; Bodnár et al. 2014; Kamakoti and Shyy 2004). Despite occurring in different degrees and forms, the FSI problem is present in several engineering systems such as engines, acoustics, turbines, pumps and others. In these systems, FSI plays an important role and influences design decisions (Bazilevs et al. 2013; Païdoussis 1998). However, systems involving FSI problems are known for their high complexity, which makes structural designs challenging and highly non-intuitive. Thus, structural optimization methods emerge as a crucial ally for the development of projects with better performance in terms of stability, stiffness and economic aspects.

Topology optimization methods have become popular in fluid–structure systems being applied to a variety of problems (Andreasen and Sigmund 2013; Vicente et al. 2015;

Responsible Editor: James K Guest

Topical Collection: 14th World Congress of Struct Multidisc Optim. Guest Editors: Y. Noh, E. Acar, J. Carstensen, J. Guest, J. Norato, and P. Ramu.

✉ R. Picelli
rpicelli@usp.br

[1] Department of Naval Architecture and Ocean Engineering, Polytechnic School of the University of São Paulo, São Paulo, Brazil

[2] Structural Engineering Department, University of California, San Diego, USA

[3] Department of Mechatronics and Mechanical Systems Engineering, Polytechnic School of the University of São Paulo, São Paulo, Brazil

[4] Department of Mining and Petroleum Engineering, Polytechnic School of the University of São Paulo, São Paulo, Brazil

Kook and Jensen 2017). Compared to parametric and shape optimization, topology optimization allows non-intuitive solutions to be generated from a full domain regardless of the initial configuration and have been adopted in several engineering areas (Bendsøe and Sigmund 2003; Zhu et al. 2021). In general, topology optimization involving multiphysics systems face higher challenges compared to the optimization of a single physics. A fundamental point to consider when optimizing FSI problems is the modeling of interface conditions. FSI problems are characterized by the strong coupling between physics, i.e., the structure and the fluid move together and depend on each other (Bungartz and Schäfer 2006; Hami and Radi 2017; Richter 2017). In some cases, the position of the FSI interface is allowed to change during optimization. This approach is called "wet" optimization. Such an approach is challenging and leads to design-dependent loads, i.e., fluid loads are intrinsically dependent on the structural boundary and can possibly change as the structural design is updated (Jenkins and Maute 2016; Lundgaard et al. 2018). Thus, it is necessary to adopt precise techniques capable of tracking coupling conditions during optimization. On the other hand, the so-called "dry" optimization does not allow the removal of interface elements and only the internal geometry of the structure is optimized (Maute and Allen 2004; Jenkins and Maute 2015). This work considers the "dry" and "wet" approach and aims to design structures with higher stiffness (minimum compliance) subject to FSI loads allowing for large displacements.

Different approaches have been used to optimize the structural topology in FSI problems. The first work employed a density-based approach. Yoon (2010) proposed a SIMP (Solid Isotropic Material with Penalization) unified model that solved both governing equations in a monolithic approach. Later, Yoon (2014) applied the same method to stress-constrained problems. Further discussions and comparisons were provided by Lundgaard et al. (2018) who revisited the same SIMP-based for FSI problems approach proposed by Yoon (2010, 2014). In both works, the "wet" optimization was considered. Density-based methods consider an interpolation in the material constant properties between solid and fluid within each element. However, such methods have an unclear structural boundaries during optimization due to the use of intermediate densities elements, which implies a difficult physical interpretation in addition to possible numerical inaccuracies. Jenkins and Maute (2015) employed a method based on the explicit level-set for "dry" optimization of FSI problems. A generalized formulation of the extended finite element method (XFEM) was used to track the changes in the structural boundary during the optimization. The same approach was applied for "wet" optimization later on (Jenkins and Maute 2016). Picelli et al. (2019) considered the level-set-based approach for fluid pressure loading problems. Fluid flooding technique was adopted to track changes in the FSI interface during optimization. A different technique for tracking the interface based on the level-set framework was proposed by Feppon et al. (2020) in the topology optimization of thermal fluid–structure problems. Feppon et al. (2020) proposed a remeshing method based on the evolution of the level-set function to capture the FSI interface. A new framework which employs reaction–diffusion equations (RDE) to update the level-set function was proposed by Li et al. (2021). In such approach, a body-fitted adaptive mesh scheme is employed as a remeshing technique. Level-set methods employ level-set functions that explicitly describe the structural boundaries via iso-contours. The interface FSI is clear and well defined. However, the level-set framework is usually complex and requires minuscious care in the level-set update to guarantee boundary smoothness, adding challenges to the already complex FSI problems.

The clear and explicit distinction between physical boundaries is also provided by binary methods (also called discrete) (Sivapuram and Picelli 2020). Alternatively, binary methods are generally easier to implement compared to level-set methods. Picelli et al. (2017) addressed the optimization of FSI problems using binary design variables via the BESO (Bi-directional Evolutionary Structural Optimization) method (Huang and Xie 2007). The fluid and solid domains as well as the governing equations were modeled separately. The BESO method, however, is built upon a heuristic-design updated scheme, presenting difficulties when applied to a general optimization problem. Still in the binary class of methods, Picelli et al. (2020a) applied the TOBS (Topology Optimization of Binary Structures) method in the "wet" optimization case of structures under fluid flow loads. The author developed a new methodology to integrate different optimization and finite element packages. The idea consists in decoupling the binary optimization grid (from TOBS) and the finite element analysis (FEA) mesh. A CAD (Computer-aided Design) model is created by reading the $\{0, 1\}$ variables and trimming the void regions (variables 0) out from the original design domain. This leads to the TOBS with geometry trimming (TOBS-GT) method. Picelli et al. (2022) showed that the TOBS-GT method can be used to optimize turbulent fluid flow properties. In this work, the idea is extended to show possible benefits in multiphysics optimization as it allows the modeling of separate domains in addition to the possibility of employing conveniently coarse meshes, decreasing the computational costs involved in the FSI simulation. The standard TOBS solver is based on formal mathematical programming which allows the efficient implementation of multiple constraints in the problem (Picelli et al. 2020b).

In such context, this work proposes the extension of the methodology based on the TOBS-GT method (Picelli et al. 2020a) for optimizing FSI problems including large

structural displacements. The TOBS is a gradient-based method and employs sequential linear approximation of objective and constraint functions to generate subproblems associated with integer linear programming (ILP). Despite the effectiveness of the studies and different approaches mentioned above, the consideration of more realistic problems including large structural deformations is still a challenging topic when dealing with FSI problems. Up to date, the design of structures under viscous fluid loads considering large displacements was effectively employed only by Jenkins and Maute (2015, 2016). When optimizing FSI problems with large structural deformations, the fluid–structure interfaces must be properly tracked and explicitly defined for sensitivities to be calculated correctly. The binary $\{0, 1\}$ design variables provide clear structures which facilitate the imposition of coupling conditions and the numerical analysis of separate fluid and structural domains. Although FSI problems are commonly transient, herein we carry out the optimization considering a steady-state regime as a design approach, since the computational costs of transient analyses are still a challenge for topology optimization. In this study, we develop a framework that extends the TOBS-GT method to efficiently deal with fluid-structure design problems considering nonlinear structural responses. Compliance minimization is solved subject to a volume fraction constraint. COMSOL Multiphysics is used as FEA package to solve FSI equations and provide semi-automatic symbolic differentiated sensitivities. An optimization grid defined by a set of binary design variables $\{0, 1\}$ is created in the TOBS module. Then, the optimization grid is passed to the FEA module and a geometry file is generated. The geometry is produced by reading the set of discrete variables, where $\{1\}$ represents the solid domain and $\{0\}$ is the void or fluid regions. The trimmed geometry is freely meshed with the FEA package. The problem is solved in the spatial (Eulerian) and material (Langragian) frame, thus allowing the map between the optimization point coordinates and the calculation of the sensitivity field in the deformed position. Fluid loads are linearly interpolated via the stress-equilibrium coupling condition. The TOBS-GT method is applied to design of 2D and 3D structures under viscous fluid flow loads. To the best author's knowledge, this is the first work to employ binary topology optimization to design FSI systems including large displacements. The remainder of the paper is as follows. Section 2 describes the FSI model used in this work: the Navier Stokes equations (Sect. 2.1), the structural mechanics (Sect. 2.2) and the coupling conditions at the interface (Sect. 2.3). The optimization problem is described in Sect. 3 including details from the TOBS and TOBS-GT methods and the computational procedure. 2D and 3D numerical examples are presented and discussed in Sect. 5. The paper is concluded in Sect. 6.

2 Fluid–structure interaction

We consider a steady-state analysis of elastic structures in contact with viscous incompressible fluid. In this work, the fluid flow is modeled in a Eulerian (spatial) frame while the solid structure is modeled in a Lagrangian (material) frame. The fluid flow is considered to be laminar and is governed by the incompressible Navier Stokes and continuity equations. Moving mesh is considered and structural nonlinear responses are evaluated.

2.1 Navier–Stokes equations

An incompressible viscous fluid flow in constant motion (as illustrated in Fig. 1) is governed by the Navier Stokes and continuity equations (Gresho and Sani 2000). Considering a steady-state incompressible homogeneous Newtonian fluid, the equations are given by

$$\rho_{\mathrm{f}}(\mathbf{v}\cdot\nabla)\mathbf{v} = \nabla\cdot[-P\mathbf{I} + \mu_{\mathrm{f}}\left(\nabla\mathbf{v} + (\nabla\mathbf{v})^{\mathrm{T}}\right)] \qquad \text{on} \quad \Omega_{\mathrm{f}}, \tag{1}$$

$$\rho_{\mathrm{f}}\nabla\cdot(\mathbf{v}) = 0 \qquad \text{on} \quad \Omega_{\mathrm{f}}, \tag{2}$$

where ρ_{f} is the fluid density, $\mathbf{v}$ is the fluid velocity, P is the fluid pressure, $\mathbf{I}$ is the unit diagonal matrix and μ_{f} is the fluid dynamic viscosity.

Equation 1 corresponds to the momentum equation in an Eulerian formulation of reference, i.e., spatial frame. The terms on the left side of the equation are due to convective acceleration and the right side represents the internal forces in the fluid (inertial forces and viscous forces). The fluid inertial and viscosity forces are related by the Reynolds number Re, where $\mathrm{Re} = F_{\mathrm{inertial}}/F_{\mathrm{viscous}}$. Equation 2 expresses the incompressibility of the fluid. In order to solve the governing fluid equations, the following boundary conditions are imposed:

$$\mathbf{v} = \mathbf{v}_0 \qquad \text{on} \quad \Gamma_{\mathrm{in}}, \tag{3}$$

$$[-P\mathbf{I} + \mu_{\mathrm{f}}\left(\nabla\mathbf{v} + (\nabla\mathbf{v})^{\mathrm{T}}\right)]\mathbf{n}_{\mathrm{f}} = -\hat{P}_0\mathbf{n}_{\mathrm{f}} \qquad \text{on} \quad \Gamma_{\mathrm{out}}, \tag{4}$$

$$\hat{P}_0 \le p_{\mathrm{out}} \qquad \text{on} \quad \Gamma_{\mathrm{out}}. \tag{5}$$

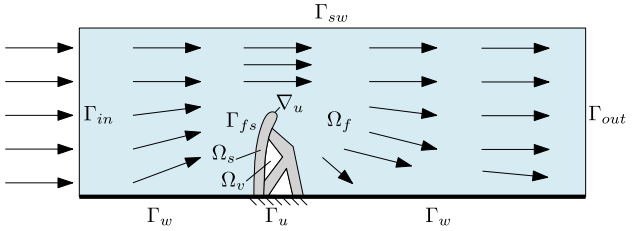

Fig. 1 A schematic illustration of the FSI problem

The inlet flow condition (Eq. 3) is prescribed the at the channel boundary Γ_{in}. At the outlet of the fluid channel Γ_{out} a stress free condition is applied (Eqs. 4 and 5), where $\mathbf{n}_{\text{f}}$ is the unit normal vector outward to the fluid and p_{out} is the pressure at the outlet of the channel. A slip condition ($\mathbf{v} \neq 0$) is imposed on the flow walls prescribed with Γ_{sw}, on the walls Γ_{w} and on the interface Γ_{fs} are assumed non-slip conditions ($\mathbf{v} = 0$).

2.2 Structural mechanics

The solid domain Ω_{s} (see Fig. 1) is computed in a Lagrangian frame (Wriggers 2008; Gatzhammer 2014). All the discrete equations are derived with respect to the original configuration of the structure (undeformed position). This formulation is commonly called Total Lagrangian formulation. In this approach, a displacement vector $\mathbf{u}$ is used to account for the displacements from each material point $\mathbf{X}$ to a spatial point $\mathbf{x}$. Thus

$$\mathbf{x} = \mathbf{X} + \mathbf{u}, \tag{6}$$

where $\mathbf{x}$ is the spatial coordinate, $\mathbf{X}$ is the material coordinate and $\mathbf{u}$ is the displacement vector. The deformation gradient tensor $\mathbf{F}$ can be introduced to report the deformation of an infinitesimal line element $\mathrm{d}\mathbf{X}$ in the material domain to a deformed line element $\mathrm{d}\mathbf{x}$ in the spatial domain as

$$\mathrm{d}\mathbf{x} = \frac{\partial \mathbf{x}}{\partial \mathbf{X}} \mathrm{d}\mathbf{X} = \mathbf{F}\mathrm{d}\mathbf{X}, \tag{7}$$

Therefore, $\mathbf{F}$ can be written as

$$\mathbf{F} = \frac{\partial \mathbf{x}}{\partial \mathbf{X}} = \nabla_{\mathbf{u}} + \mathbf{I}, \tag{8}$$

where $\nabla_{\mathbf{u}}$ is the displacement gradient given by the derivatives of the deformed coordinates with respect to the initial coordinates. The strain state is evaluated in the material configuration by the Green–Lagrange strain tensor given by

$$\mathbf{E} = \frac{1}{2}(\mathbf{C} - \mathbf{I}), \tag{9}$$

where $\mathbf{C} = \mathbf{F}^{\text{T}}\mathbf{F}$ is the right Cauchy–Green deformation tensor. The tensors $\mathbf{E}$ and $\mathbf{C}$ do not contain rigid body strains. The strain tensor $\mathbf{E}$ can be rewrite using the displacement gradient $\nabla_{\mathbf{u}}$ as

$$\mathbf{E} = \frac{1}{2}[(\nabla_{\mathbf{u}})^{\text{T}} + \nabla_{\mathbf{u}} + (\nabla_{\mathbf{u}})^{\text{T}}\nabla_{\mathbf{u}}], \tag{10}$$

where the higher-order term $(\nabla_{\mathbf{u}})^{\text{T}}\nabla_{\mathbf{u}}$ corresponds to the nonlinear character. The equilibrium state is described in terms of the 2nd Piola–Kirchhoff stress tensor $\mathbf{S}$ defined as

$$\nabla \cdot (\mathbf{FS}) + \mathbf{f}^{fsi} = 0, \tag{11}$$

where $\mathbf{f}^{fsi}$ is the vector of fluid loads applied on the structure, i.e., at the interface Γ_{fs}. The stress tensor $\mathbf{S}$ can be related with the Cauchy stress tensor $\boldsymbol{\sigma}_{\text{s}}$ via

$$\boldsymbol{\sigma}_{\text{s}} = \mathbf{JFSF}^{\text{T}}, \tag{12}$$

where $\mathbf{J}$ is the Jacobian matrix. Once the material is considered to be isotropic and linearly elastic, the linear constitutive relation between the stress tensor $\mathbf{S}$ and the strain tensor $\mathbf{E}$ can be expressed by the Saint-Venant Kirchhoff elastic constitutive equation which is stated by

$$\mathbf{S} = \lambda_{\text{s}}(\text{tr}\mathbf{E})\mathbf{I} + 2\mu_{\text{s}}\mathbf{E}. \tag{13}$$

where λ_{s} and μ_{s} are Lamé constants. This constants can be described in terms of the Young's modulus E and Poisson's ratio ν as

$$E = \frac{\mu_{\text{s}}(3\lambda_{\text{s}} + 2\mu_{\text{s}})}{\lambda_{\text{s}} + \mu_{\text{s}}}, \tag{14}$$

$$\nu = \frac{\lambda_{\text{s}}}{2(\lambda_{\text{s}} + \mu_{\text{s}})}. \tag{15}$$

In order to solve Eq. 11, Dirichlet boundary conditions are applied at Γ_{u} as

$$\mathbf{u} = 0 \qquad \text{on} \quad \Gamma_{u}. \tag{16}$$

2.3 Coupling interface

The coupling between solid domain and fluid domain at the FSI interface is defined by the kinematic and stress equilibrium conditions. The kinematic condition concerns the continuity in velocity and the stress equilibrium condition defines the continuity of the interface with respect to the normal vectors of both domains (Lund et al. 2003). The stress coupling condition for steady-state is expressed as

$$\boldsymbol{\sigma}_{\text{s}}\mathbf{n}_{\text{s}} = -\boldsymbol{\sigma}_{\text{f}}\mathbf{n}_{\text{f}} \qquad \text{on} \quad \Gamma_{fs}. \tag{17}$$

where $\boldsymbol{\sigma}_{\text{s}}$ is the solid stress tensor, $\boldsymbol{\sigma}_{\text{f}}$ is the fluid stress tensor, $\mathbf{n}_{\text{s}}$ is normal unit vector outward to the solid and $\mathbf{n}_{\text{f}}$ is normal unit vector outward to the fluid, both in the deformed configuration. A moving mesh is considered in order to evaluate the motion of the fluid–structure interface, i.e., how the structure deforms due to fluid flow loads and how the fluid domain changes due to the motion of the structural boundary. The moving mesh interface in COMSOL Multiphysics employs the Arbitrary Lagrangian–Eulerian (ALE) method which separates the spatial frame (fluid domain) from the material frame (solid domain), enabling the easy identification of changes in physical boundaries. In this way, the solid structure follows the mesh displacement.

3 Topology optimization problem

3.1 Problem formulation

This study concerns the structural mean compliance minimization subject to a volume fraction constraint. The mathematical formulation of the problem considering binary variables $\{0, 1\}$ can be stated as

$$\begin{aligned} &\underset{\rho}{\text{Minimize}}\ C(\boldsymbol{\rho}) = \frac{1}{2}\mathbf{f}^{\mathrm{T}}\mathbf{u} \\ &\text{Subject to } V(\boldsymbol{\rho}) \leq \overline{V}, \\ &\qquad \rho_j \in \{0,1\},\ j \in [1, N_d], \end{aligned} \tag{18}$$

where $\boldsymbol{\rho}$ represents the vector of design variables ρ_j, $C(\boldsymbol{\rho})$ is the structural mean compliance or total deformation energy, $\mathbf{f}$ and $\mathbf{u}$ corresponds to the loads vectors and the global structural displacement, respectively, V is the total material volume of the structure, $\overline{V}$ is the prescribed structural volume fraction and N_d is the number of elements in the design variables vector.

3.2 Material models

In order to evaluate the derivatives of the structural mean compliance, the physical model should be interpolated with the design variables. We adopted the SIMP material model which is expressed as

$$E(\rho_j) = \rho_j^p E_0 \qquad \text{on} \qquad \Omega_s, \tag{19}$$

where $E(\rho_j)$ is the interpolated material property with respect to the design variable ρ_j, E_0 is the Young's modulus of the solid element and p is the penalty exponent factor. We also adopted a linear material interpolation in order to couple the sensitivities with the fluid loads that change during optimization with the material removal from the fluid–structure interface. Thus, the Eq. 17 referring to the stress equilibrium condition is rewritten as

$$\boldsymbol{\sigma}_{\mathrm{s}}\mathbf{n}_{\mathrm{s}} = -\rho_j\boldsymbol{\sigma}_{\mathrm{f}}\mathbf{n}_{\mathrm{f}} \qquad \text{on} \qquad \Gamma_{fs}. \tag{20}$$

More information and discussions about the effects of this material model are given in the numerical results (Sect. 5).

3.3 TOBS method

The standard TOBS method generates optimization subproblems via sequential linear approximation. Since binary design variables $\{0, 1\}$—0 for void and 1 for solid material—are employed, the TOBS framework solves the linear optimization subproblems using integer linear programming (ILP). Therefore, in order for the design variables to remain integer and binary during optimization and the ILP problem to be satisfied, changes in the design variables are constrained by means of a bounded constraint described by

$$\begin{cases} 0 \leq \Delta\rho_j^k \leq 1 & \text{if } \rho_j^k = 0, \\ -1 \leq \Delta\rho_j^k \leq 0 & \text{if } \rho_j^k = 1, \end{cases} \tag{21}$$

where $(\cdot)^k$ indicates the value of quantity $(\cdot)$ at iteration k and $\Delta\boldsymbol{\rho}^k$ is the vector of changes in the design variables. To keep the binary nature of problem the changes in the design variables are restricted. Therefore, for a solid element ($\rho_j = 1$) the possible changes are $\{0\}$ or $\{-1\}$ which remains solid or becomes void, respectively. For void elements the same definition is valid, where $\{0\}$ is prescribed to remain void element or $\{1\}$ to become a solid element. The optimization subproblems are generated applying Taylor's series approximation and truncating at the linear terms. The objective and constraint functions can be rewritten as

$$\begin{aligned} C(\boldsymbol{\rho}) &\approx C(\boldsymbol{\rho}^k) + \frac{\partial C(\boldsymbol{\rho}^k)}{\partial \boldsymbol{\rho}} \cdot \Delta\boldsymbol{\rho}^k + O(\left|\left|\Delta\boldsymbol{\rho}^k\right|\right|_2^2), \\ V(\boldsymbol{\rho}) &= V(\boldsymbol{\rho}^k) + \frac{\partial V(\boldsymbol{\rho}^k)}{\partial \boldsymbol{\rho}} \cdot \Delta\boldsymbol{\rho}^k, \end{aligned} \tag{22}$$

where $O(\left|\left|\Delta\boldsymbol{\rho}^k\right|\right|_2^2)$ represents the truncation error. There is no error associated with the volume function because its variation is linear. In Eq. 22 the higher-order terms for the mean compliance function are neglected since the ILP problems are created using linear approximation. This implies that, for the approximation to be valid, the truncation error needs to be small enough. For this, an extra constraint is added to constrain the number of changes to the design variables in each iteration. This constraint can be expressed as

$$\left|\left|\Delta\boldsymbol{\rho}^k\right|\right|_1 \leq \beta N_d. \tag{23}$$

In the context of topology optimization, the β parameter guarantees that only a fraction of the total number of variables evolves from solid $\{1\}$ to empty $\{0\}$ and vice versa in each iteration. Therefore, the adoption of small β values is essential for the truncation error to be small enough.

Thus, the linearized optimization subproblem can be written as

$$\begin{aligned} &\underset{\Delta\boldsymbol{\rho}^k}{\text{Minimize}}\ \frac{\partial C(\boldsymbol{\rho}^k)}{\partial \boldsymbol{\rho}} \cdot \Delta\boldsymbol{\rho}^k, \\ &\text{Subject to } \frac{\partial V(\boldsymbol{\rho}^k)}{\partial \boldsymbol{\rho}} \cdot \Delta\boldsymbol{\rho}^k \leq \overline{V} - V\left(\boldsymbol{\rho}^k\right) := \Delta V^k, \\ &\qquad \left|\left|\Delta\boldsymbol{\rho}^k\right|\right|_1 \leq \beta N_d, \\ &\qquad \Delta\rho_j^k \in \{-\rho_j^k, 1-\rho_j^k\},\ j \in [1, N_d], \end{aligned} \tag{24}$$

where $\Delta\rho_j^k$ is the update of the kth design variable corresponding to the jth element and ΔV^k is the upper limit of the

volume constraint. Solving the ILP problem, the design variables are updated as

$$\boldsymbol{\rho}^{k+1} = \boldsymbol{\rho}^{k} + \Delta\boldsymbol{\rho}^{k}. \tag{25}$$

As mentioned earlier, the linear approximation of functions is only valid for small changes in the objective and constraint functions at each update of the design variables. However, some of the problem's constraints can start in an infeasible space due to the bound $\Delta V_i^k = \overline{V} - V\left(\boldsymbol{\rho}^k\right)$ requiring a big step to reach a viable solution. Since the topology change is restricted to each iteration by the β parameter, the upper bounds of the constraints ΔV^k are relaxed to generate feasible ILP subproblems. The constraint bounds are relaxed using

$$\Delta V^k = \begin{cases} -\epsilon_i V\left(\boldsymbol{\rho}^k\right) & : \overline{V} < (1-\epsilon_i)V\left(\boldsymbol{\rho}^k\right), \\ \overline{V} - V\left(\boldsymbol{\rho}^k\right) & : \overline{V} \in [(1-\epsilon_i)V\left(\boldsymbol{\rho}^k\right), (1+\epsilon_i)V\left(\boldsymbol{\rho}^k\right)], \\ \epsilon_i V\left(\boldsymbol{\rho}^k\right) & : \overline{V} > (1+\epsilon_i)V\left(\boldsymbol{\rho}^k\right), \end{cases} \tag{26}$$

where ϵ_i is the relaxation parameter corresponding to the volume constraint. Effectively, the parameter ϵ gradually limitates the constraint functions moves towards their upper bounds ensuring that a viable solution exists at each iteration.

The ILP problem (Eq. 24) originated from the sequential linearization of functions is the same as a linear programming (LP) problem; however ILP problems are restricted to integer design variables. Therefore, ILP-based solutions can be slightly below the solutions generated by LP problems. However, the structural design obtained by ILP solutions has a clear and well-defined boundary/interface due to the use of integer variables. A famous technique used to solve ILP problems is the branch-and-bound algorithm. In this technique, the ILP problem is initially solved as an LP problem, i.e., without integer constraints. Then, the obtained solution is used as the initial solution and different LPs are created with additional extra limits on the design variables, which forces the optimizer to generate entire solutions in the branches (Land and Doig, 1960). In this work, we employ the branch-and-bound algorithm present in the CPLEX package to solve the ILP problem generated at each iteration.

3.4 Sensitivity analysis

3.4.1 Adjoint sensitivities

The TOBS is a gradient-based optimization method, hence the gradients (sensitivities) of the objective and constraint functions are required to iterate over solutions. The respective sensitivities can be calculated using the adjoint method (Haftka and Gürdal 1991; Bendsøe and Sigmund 2003). The general formulation of the adjoint equation for a Lagrangian functional can be given by

$$\left(\frac{\partial \mathbf{R}}{\partial \mathbf{u}}\right)^{\mathrm{T}} \boldsymbol{\lambda} = -\left(\frac{\partial f}{\partial \mathbf{u}}\right)^{\mathrm{T}}, \tag{27}$$

where $\boldsymbol{\lambda}$ corresponds to the vector of adjoint variables, f is the vector of objective function and $\mathbf{R}$ is the residual. Sensitivities can then be calculated by the following expression

$$\left(\frac{\mathrm{d}L}{\mathrm{d}\boldsymbol{\rho}}\right) = \left(\frac{\partial f}{\partial \boldsymbol{\rho}}\right)^{\mathrm{T}} + \boldsymbol{\lambda}^{\mathrm{T}} \frac{\partial \mathbf{R}}{\partial \boldsymbol{\rho}}. \tag{28}$$

The structural mean compliance sensitivities are then calculated by the generic function (Eq. 28). The structural volume sensitivities with respect to the design variable ρ_j are expressed as

$$\frac{\partial V}{\partial \rho_j} = V_j, \tag{29}$$

where V_j is the volume fraction referring to the design variable j.

4 Computational procedures

The proposed method considers the optimizer and problem physics in a decoupled way, i.e., as independent modules. A geometry trimming procedure and interpolation of sensitivities are used to integrate both modules. The proposed optimization method is based on material distribution and built upon the standard TOBS method (Sivapuram and Picelli 2018). A diagram illustrating the steps of the algorithm is presented in Fig. 3. The equilibrium equations of the FSI problem are solved via the finite element method using an external FEA package, herein COMSOL Multiphysics. The equations are computed with a segregated numerical solver, i.e., with separate domains and in a iteratively manner. In addition, the required sensitivities for optimization are also provided by the FEA package. Besides the fluid–structure interaction module used for the physical analysis of the problem in COMSOL Multiphysics, we employed the topology optimization module to include the material model into the design domain. Through the "density model" tool present within the topology optimization module we can define the type of interpolation and the penalty factor as well. Also, the "optimization" module is used to access the semi-automatic built-in symbolic differentiation tool. The interpolation of the material and FSI coupling (Eqs. 19 and 20) is determined by editing the properties in the structural mechanics and multiphysics coupling modules. Sensitivity analysis is performed by the adjoint method and obtained via the semi-automatic built-in symbolic differentiation

module integrated in the software. The TOBS approach with geometry trimming (GT), so-called TOBS-GT, uses a grid points of interest described by binary variables $\{0, 1\}$ to communicate with the FEA module. Geometry trimming (GT) method is the process of creating a CAD geometry by reading the design variables provided and trimming out the initial CAD model of the design domain. The procedure reads the binary design variables—which prescribes the presence (1) or absence (0) of material—and generates a CAD model which contains all the contour information of the problem. This procedure is illustrated in Fig. 2.

A geometry is produced from these contour information (in .dxf, for 2D, or .stl format, for 3D) and transferred to the FEA module via the geometry trimming technique. The optimization grid as well as the .dxf and .stl files are dimensionless. Therefore, a scale factor is applied in order to obtain the actual physical dimension of the problem. The void domains described by variables 0 are trimmed out from the design domain and the CAD file with the respective geometry is updated every iteration. The contour information contains the exact location of the void regions (holes), i.e., whether they are located entirely inside the solid design domain or at the FSI interface. Internal holes are completely trimmed out from the CAD model and holes at the initial FSI interfaces are assigned to be fluid domain. Thus, the FSI interface is directly tracked and the "fluid flooding" technique as previously used in the literature (Picelli et al. 2015) is not needed. In this work, we do not apply smoothing filters on the FSI interface, so the topologies have a staircase contour. Once the fluid and solid domain is defined, COMSOL Multiphysics are able to identify the boundaries corresponding to FSI interfaces and apply the coupling conditions. The software meshes the geometry freely according to physical requirements. The use of free finite element meshes configured according to physical requirements is advantageous for fluid structure problems, since the mesh quality at the physical boundaries—flow channel walls and FSI interface—are higher, promoting a good approximation of the problem. In this study, this procedure is done using the option `physics controlled` in COMSOL Multiphysics. Triangular and quadrilateral elements are employed. The analyses are performed assuming plane strain. A quadratic Lagrange approximation is used for the structural analysis and the $P_1 + P_1$ or $P_2 + P_1$ discretization is employed for the fluid flow. FEA is carried out and semi-automatic differentiated sensitivities are computed. The Fluid–Structure Interaction interface in COMSOL Multiphysics employs an arbitrary Lagrangian–Eulerian (ALE) method to account for changes in physical boundaries. The ALE method integrates the fluid flow domain using a spatial frame (Eulerian description) with the solid domain using a material frame (Lagrangian description). The spatial frame is formulated in a system of fixed coordinates in space and the material frame is fixed to the material and moves along with the deformed object. The optimization grid is defined in the material frame and sensitivities are computed in the deformed structural position, as illustrated in Fig. 4. An auxiliary linear analysis is considered in order to avoid convergence problems arising from large local structural displacements due to possible breakage of thin structural members. In summary, the system is analyzed first in the nonlinear regime and, if by any chance the solver does not converge, we employ a linear analysis in the current iteration in order to re-establish the stability of the

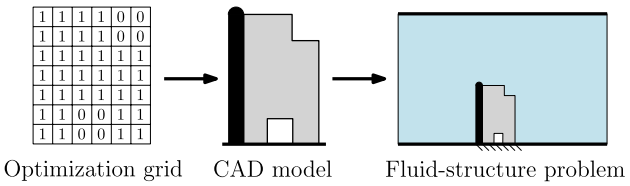

Fig. 2 Representation of the geometry trimming (GT) procedure

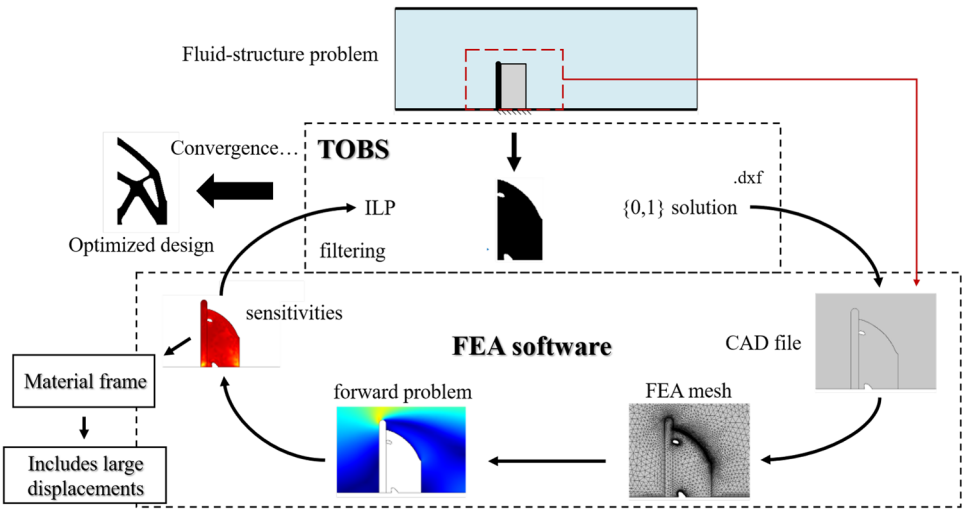

Fig. 3 Illustration of the TOBS-GT method for fluid–structure design including large displacements

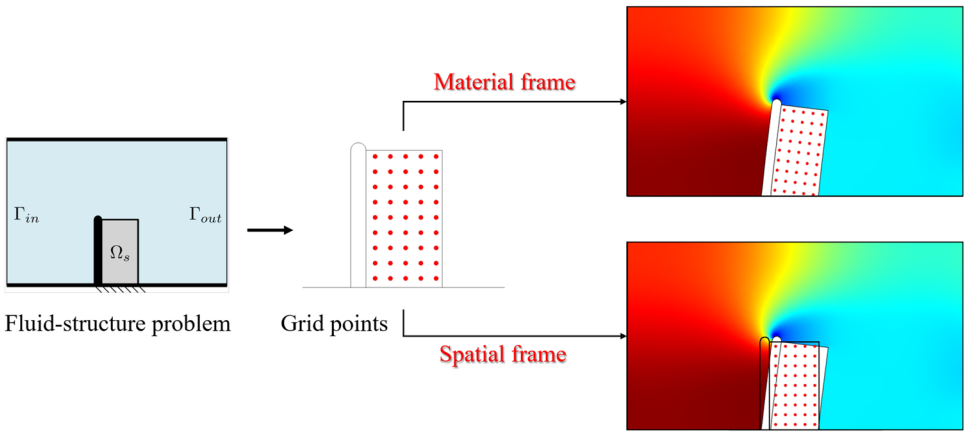

Fig. 4 TOBS optimization grid computed in the material frame with mapping to the spatial frame

structure and move on with the optimization. In this work, linear analysis was activated only in a few iterations, not being necessary in all examples. Furthermore, all problems converged within the nonlinear regime.

The objective function of the structural mean compliance is computed through the expression `solid.Ws_tot` incorporated in COMSOL Multiphysics. The sensitivities of the structural model are integrated in the variable `fsens(dtopo1.theta_c)/dvol`, where `theta_c` is the vector of interpolation variables (Eqs. 19 and 20) and `dvol` is a volume factor variable considered due to the different sizes of the finite elements. The sensitivities computed at each point are extracted through a set of grid points coincident with the optimization grid. In the TOBS module, a spatial filter is applied to the sensitivities to smooth out the problem and avoid numerical problems, such as the checkerboard. With the respective sensitivities the optimizer provides a new set of binary variables $\{0, 1\}$. This process is repeated until convergence. A summary of the main steps for the TOBS-GT approach is presented below:

1. Define the TOBS parameters;
2. Initialize design variables in the TOBS module via the optimization grid $\{0, 1\}$;
3. Generate a CAD geometry in the FEA package by reading the optimization grid variables and trimming out the void regions;
4. Mesh the geometry created by the CAD model;
5. Solve the FSI system governing equations;
6. Compute the semi-automatic differentiated sensitivities in the grid points considering the mapping between the material and spatial frames;
7. Extract the calculated sensitivities and transfer them to the TOBS module;
8. Filter the sensitivity field defined in the grid points;
9. Solve the ILP problem and update the design variables $\{0, 1\}$ in the optimization grid;
10. Evaluate the convergence of the problem. If converged, stop. Otherwise, return to step 3.

5 Numerical examples

This section presents the results obtained using the TOBS-GT method. The goal is to minimize the mean compliance of structures under viscous fluid flow loads including large displacements subject to a volume fraction constraint. The first problem is a variation on a well-known example in the literature called "the wall" problem. We solve the problem by optimizing only the internal geometry of the structure, i.e., "dry" optimization. In the second case, the "wet" optimization approach is considered for a second variation of "the wall" example. In order to compare results, in the first two examples the problem is solved considering the small and large displacements. The third problem presents the application of the method in 3D problems. The numerical examples shown in the following sections were computed using the Intel Xeon Silver 4114 - 2x CPU 2.20 GHz - 128GB RAM. In all the examples, the convergence is defined by averaging the changes in the mean compliance function over 6 consecutive iterations for a tolerance of $\tau = 0.001$.

5.1 The wall—"Dry" optimization

The first problem consists of a solid wall immersed in a fluid flow rectangular channel, as shown in Fig. 5. In this problem, we analyze the same problem considering small

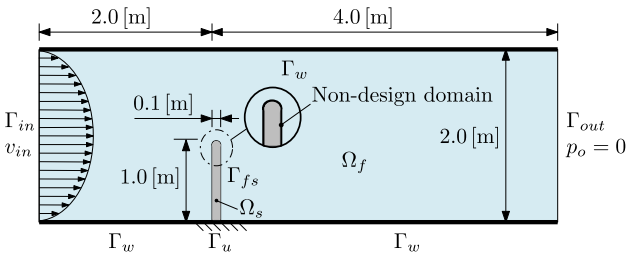

Fig. 5 The wall problem: "Dry" optimization

and large displacements for comparison purposes. We seek to optimize the "dry" topology of the wall, i.e., the internal geometry. The properties of the solid material are Young's modulus $E_0 = 400$ kPa and Poisson's ratio $\nu = 0.3$. The fluid density is $\rho_f = 1\,\text{kg/m}^3$ and dynamic viscosity $\mu_f = 1$ Pa s. The average inlet velocity is defined by the Reynolds number described by $\text{Re} = \rho_f v_{in} D/\mu_f$, where ρ_f is the fluid density, v_{in} is the mean inlet velocity, D is channel height and μ_s is the fluid dynamic viscosity. Herein, we assume $\text{Re} = 1$. The flexible solid wall is immersed in a rectangular channel of 6×2 m and it is subject to viscous fluid flow loads. This example is similar to the proposed by Jenkins and Maute (2015). The fluid flow is prescribed with a parabolic velocity profile at the channel inlet described by $\mathbf{v} = v_{in} 6(H - y)y/H^2$ where H is the height of the fluid channel and y is the coordinate in the y direction at each point of the inlet. In the outflow a stress free condition is enforced (with $p_{out} = 0$). A non-slip condition is imposed on all walls of the fluid channel. The bottom edge of the structure is fixed; the displacements are $\mathbf{u} = \mathbf{0}$ on this edge. A layer of passive elements (non-design domain) with a thickness of 0.01 m is assumed between the interface and the design domain (see Fig. 5).

The internal wall topology is optimized using the TOBS-GT method. The goal of the problem is to minimize the mean compliance of the structure subject to a volume fraction constraint of $\bar{V} = 60\%$. A 50×500 optimization grid is employed for optimization. A filter radius of 10 grid sizes is adopted. Material model is interpolated considering $p = 3$. The constraint relaxation parameter ϵ is set as 0.01, i.e., the volume function changes 1% at each iteration until it approaches the prescribed volume fraction constraint $\bar{V}$. The truncation parameter—that restricts the percentage of change in design variables at each iteration—is set as $\beta = 0.02$. Figure 6 presents the snapshots of the iterations along the optimization loop for the two cases, the black region represents the solid (1) and the white region corresponds to void (0).

The inclusion of the structural nonlinear response leads to obtaining a different optimized design compared to the linear problem. Figure 6 shows the material distribution within the design domain during the optimization process. Thin bars (similar to a truss) form along the iterations. As expected, the internal arrangement of the bars in the optimized design of each case differs. In the first case—Fig. 6a—the optimized design has a larger amount of bars being these of smaller thickness and in the second case—Fig. 6b—there are fewer bars with greater thickness. A larger portion of the material is distributed close to the clamped boundary in both cases in order to reduce the overall deformation of the structure. The optimized design obtained for large displacements—Fig. 6b—is similar to the topology obtained by Jenkins and Maute (2015).

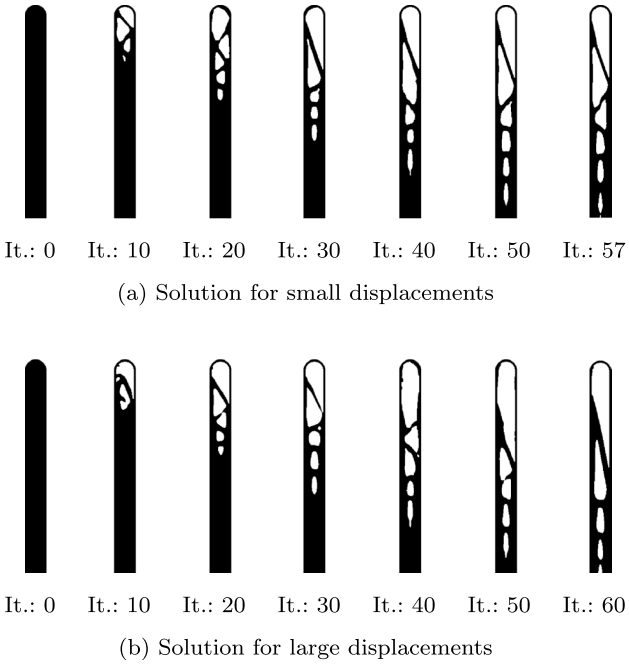

(a) Solution for small displacements

(b) Solution for large displacements

Fig. 6 Topology snapshots along the optimization process for the different cases: **a** considering small structural displacements and **b** considering large structural displacements. The black region represents solid (1) and the white region corresponds to void (0)

The fluid velocity and pressure fields of the optimized design are plotted in Fig. 7 for the two cases. Velocity profiles and pressure fields are similar in the small and large displacement cases. In general, a greater magnitude in the velocity profile it is just above the structure (see Fig. 7a, c). In the pressure fields—Fig. 7b, d—it is possible to notice a high positive pressure on the left side of the structure and a significantly lower pressure on the right side, in addition to the existence of a small region of negative pressure coupled in the back of the structure. However, despite the similarity, the case considering small displacements reaches higher pressure values, as shown in Fig. 7b. In addition, because the FSI interface remains the same along the optimization process, the design obtained for this case would be similar to a case considering a static distributed load—similarly as used in buildings design—since the fluid loads act as a distributed load over the entire interface of the structure. In the large displacements case, a larger deformation is observed at the top of the structure since the greatest amount of material is distributed at the bottom of the domain. The mapping and distinction between the material and spatial frames in the fluid–structure model allows the TOBS-GT optimization grid to be computed following the deformation of the structure. Structural displacements are computed by the FEA package and the displacement vector is added to the coordinates of the solid material. The optimization grid points are fixed to this frame of reference and the sensitivities are

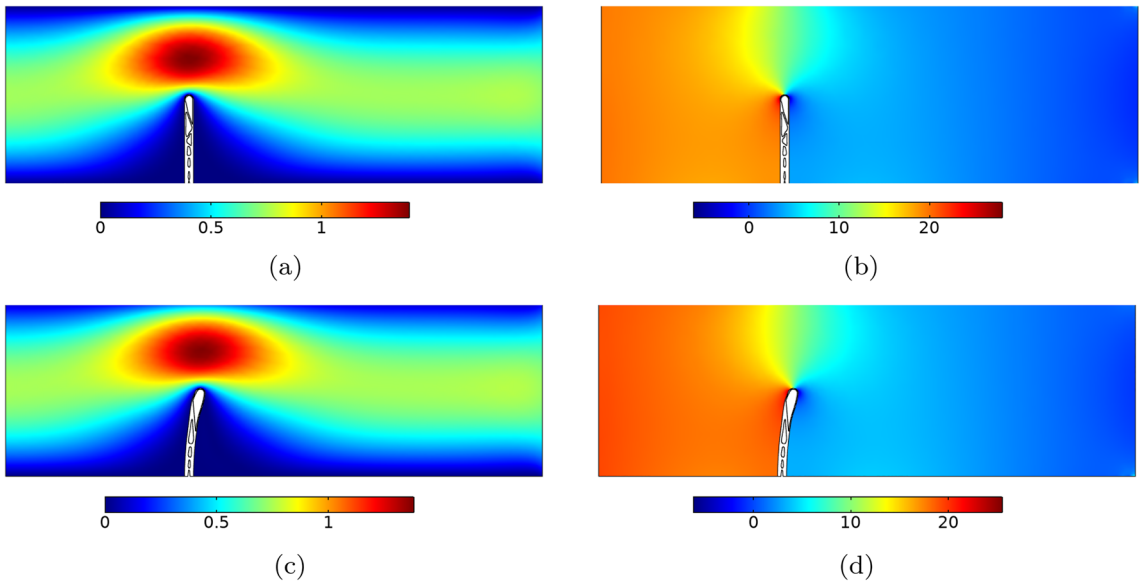

Fig. 7 Velocity magnitude (in m/s) and pressure field (in Pa) for the optimized designs: **a**–**b** considering linear regime and **c**–**d** considering nonlinear regime

computed accordingly. In this example, the linear interpolation loads does not influence the obtained solutions since only the "dry" topology is optimized, i.e., the solid elements at the interface—in contact with the fluid flow loads—remain in the same position throughout optimization.

The evolutions of the objective (mean compliance) and constraint (volume) functions are presented in Fig. 8. As seen in the history of the structural volume fraction, the removal of elements is done gradual as established by the parameter ϵ. It is possible to notice some jumps in the evolution of the objective function in both cases. These punctual increases in the objective function are due to the breakage of the thin bars along the iterations, which causes large local structural deformation, generating a significant increase in compliance, as illustrated in the colorized snapshots with the velocity field presents in Fig. 8a, b. However, this behavior does not occur in all cases. The occasional increase in the evolution of the mean compliance is also observed by Jenkins and Maute (2015). Furthermore, it is interesting to note that with the breakage of the thin bars and consequently the increase in local deformation, the optimizer seeks to add material in order to reduce large deformations and, consequently, minimize compliance. The problem considering small displacements (linear regime) converges to a structural mean compliance value of 0.0514 Nm in 57 iterations. While the final design optimized considering large displacements (nonlinear regime) is achieved in 60 iterations with a structural compliance value of 0.0543 Nm.

5.2 The wall—"Wet" optimization

In this example, a flexible solid wall is immersed in a fluid flow channel, as shown in Fig. 9. We apply the TOBS-GT method for the optimization of the "wet" topology. This is a classic example of the literature, first proposed by Yoon (2010), explored later by other authors (Picelli et al. 2017; Li

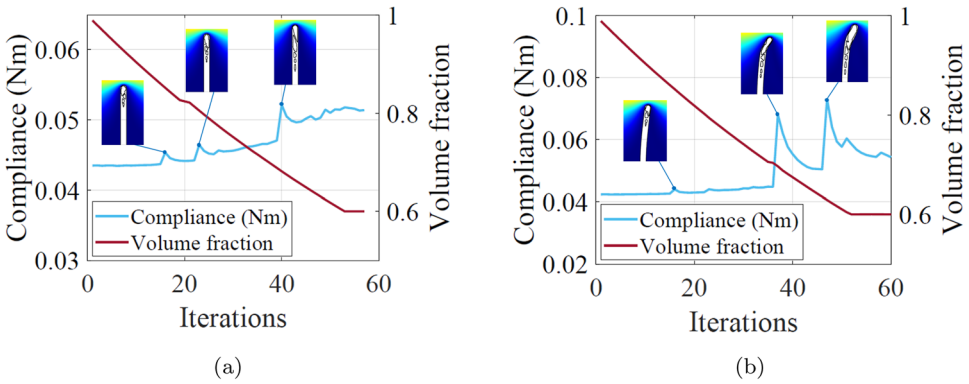

Fig. 8 Evolution history of objective function and constraint function for the case considering **a** small displacement and **b** large displacements

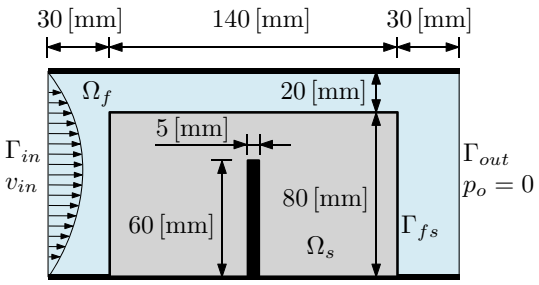

Fig. 9 The wall problem: "Wet" optimization

et al. 2021). A variation of the problem with a larger design domain was proposed by Lundgaard et al. (2018). Herein, we revisit this problem including larger displacements. The objective is to solve the minimization of the structural mean compliance subject to a volume fraction constraint. In comparison to Lundgaard et al. (2018), we slightly increased the height of the non-design domain bar to obtain larger deformation. The physical properties adopted for the solid domain are Young's modulus $E_0 = 1$ Pa and Poisson's ratio $\nu = 0.3$. The fluid is water, i.e., with density $\rho_f = 1000$ kg/m^3 and dynamic viscosity $\mu_f = 0.001$ Pa s. The average inlet velocity is defined by the Reynolds number, which is Re = 80.

The fluid flow enters the left edge of the channel with a normal parabolic velocity profile. At the exit of the channel the pressure condition $p_{\text{out}} = 0$ is imposed. On the walls of the fluid flow channel, a non-slip condition is prescribed. The structure is fixed on bottom boundary, i.e., the displacements are $\mathbf{u} = \mathbf{0}$. The objective of this example is to design an aerodynamic support within a 140×80 mm domain, where a passive region (non-design domain) corresponding to a mid-solid barrier is assumed. Structural mean compliance is minimized via the TOBS-GT method subject to final volume fraction of 10%. A 280×160 optimization grid size is used for the design domain. In regard to optimization coefficients, the constraint relaxation parameter is set to $\epsilon = 0.02$, the truncation error constraint parameter to $\beta = 0.05$, and a filter radius of 12 grid sizes. The problem is analyzed for small and large structural displacements. Figure 10 presents the topology design, velocity and pressure fields of both cases for the optimized problem using $p = 5$.

It can be noticed that for the large displacement case most of the material is deposited on the left side of the structure (see Fig. 10d) while in small displacement problem the distribution of solid material within design domain is done in a more balanced way, as seen in Fig. 10a. The velocity and pressure fields differ in the two cases, with higher values observed for the small displacements study. The optimized topology in the small displacement solution is obtained in 122 iterations with the global structural mean compliance value of 1.534×10^{-8} Nm. A cross-comparison between both designs obtained is presented in Table 1. Curiously,

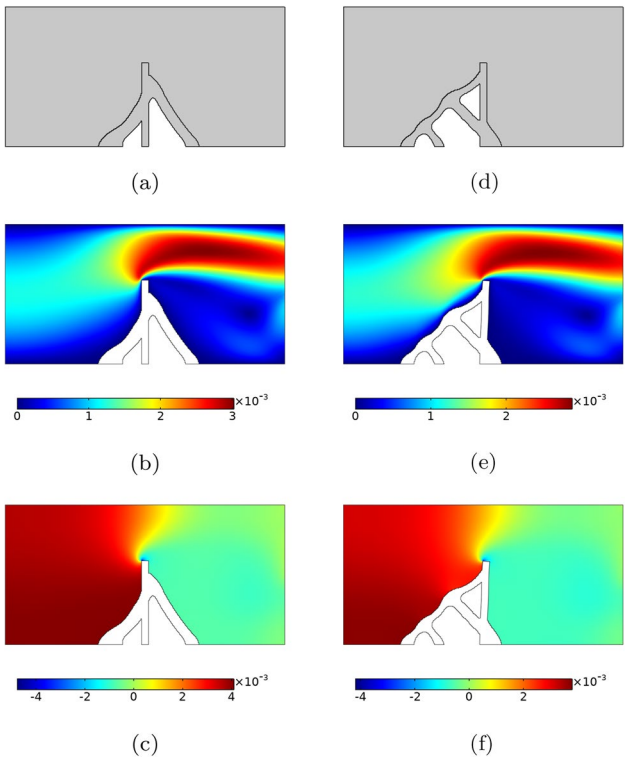

Fig. 10 Comparison between the optimized design obtained considering **a**–**c** small and **d**–**f** large displacements: **a** and **d** topology design, **b** and **e** velocity magnitude (in m/s), **c** and **f** pressure field (in Pa) using $p = 5$

the design obtained from the optimization including the geometric nonlinearity presents a higher performance for both cases, i.e., with and without considering the nonlinearities. From this, the advantages of modelling large deformation can be evidenced, but further investigations are necessary to explain why the linear design was not able to find a better solution.

In order to verify the influence of the penalty factor p, the problem is solved for three different penalty factors $p = \{3, 5, 10\}$ considering large displacements. The velocity and pressure fields are plotted in Fig. 11 for the three cases. It is possible to notice that the optimized structural designs are different for the studied penalty factors. In this model, lower penalty factors favour both stiffness and fluid loading interpolation, while larger penalties decrease considerably the calculation of the fluid loading in the sensitivities. This is also discussed in Yoon (2010) and Lundgaard et al. (2018). As seen in Fig. 11, more material was deposited on the left side of the structure when lower penalty factors ($p = 3$ and 5) were used. This fact is because with the interpolation of fluid loads, the optimizer is able to work on reducing the high pressure and shear loads arising from the direct contact of the fluid flow with the solid structure. In fact, the structure obtained using $p = 3$ presents the lowest mean compliance

Table 1 Cross-comparison between designs obtained considering small and large displacements

Designed for/simulated for	Small displacements	Large displacements
Small displacements 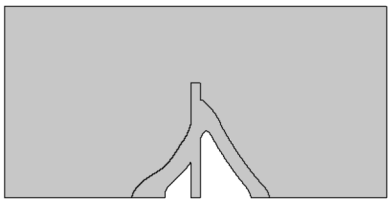	$C(x) = 1.5337 \times 10^{-8}$ Nm	$C(x) = 1.5290 \times 10^{-8}$ Nm
Large displacements 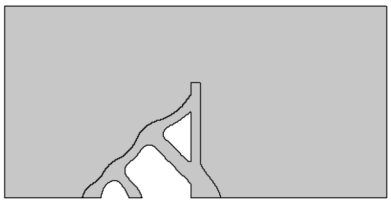	$C(x) = 1.0695 \times 10^{-8}$ Nm	$C(x) = 1.1177 \times 10^{-8}$ Nm

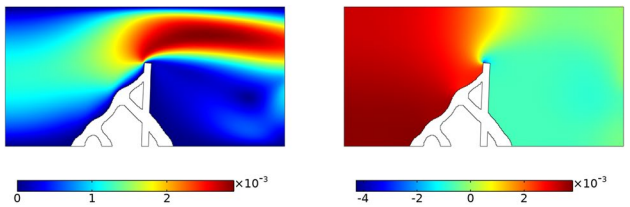

(a) $p = 3$, $C(x) = 1.0455{\cdot}10^{-8}$ Nm

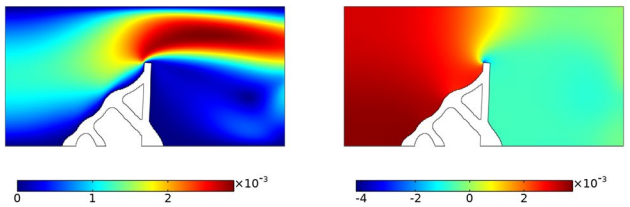

(b) $p = 5$, $C(x) = 1.0695{\cdot}10^{-8}$ Nm

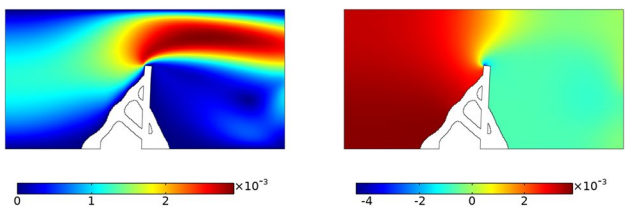

(c) $p = 10$, $C(x) = 1.0990{\cdot}10^{-8}$ Nm

Fig. 11 Velocity fields in m/s (left side) and pressure in Pa (right side) of the topology optimized for $p = \{3, 5, 10\}$

value between the three designs. When solving the problem using $p = 10$, more material was deposited closer to the mid-solid wall. Our numerical experience tells that FSI examples with high pressure and shear loads such as this one present convergence difficulties if the fluid loading sensitivities are not used, especially for higher Reynolds number. The structural members in the three designs are arranged to globally reduce the load. The velocity and pressure fields are similar in the three cases. The fluid flow velocity reaches a significant magnitude near the upper region of the intermediate barrier. Besides, the pressure field varies from positive to negative values in after the flow passes the obstacle. Figure 12 shows the evolution of the topology and velocity profile over the iterations for the case of $p = 5$. As it can be observed during optimization a clear and explicit distinction between physical boundaries—solid and fluid—is obtained along all iterations due to the binary variables.

The evolution history of the mean compliance and volume fraction functions are shown in Fig. 13. The history of the objective function presents some peaks, similarly as in the example of the optimization of the "dry" topology 5.1. Sudden increases in compliance were also observed by Jenkins and Maute (2016) in "wet" topology optimization problems. The global measure of structural mean compliance is minimized and the final obtained values are lower than the initial ones. Clear and explicit optimized topologies are obtained. The mesh created by COMSOL Multiphysics for the optimized FSI design using $p = 5$ including the fluid domain is shown in Fig. 14. The area delimited in red represents the initial design domain. The CAD geometry trimming allows the meshes to be freely created, meeting the physical requirements. As it can be noticed, the mesh has a larger discretization in the FSI boundaries and quadrilateral elements are used in the fluid walls. The finite element mesh is composed of 15,197 elements—14,637 triangular and 560 quadrilateral elements—while the TOBS-GT optimization

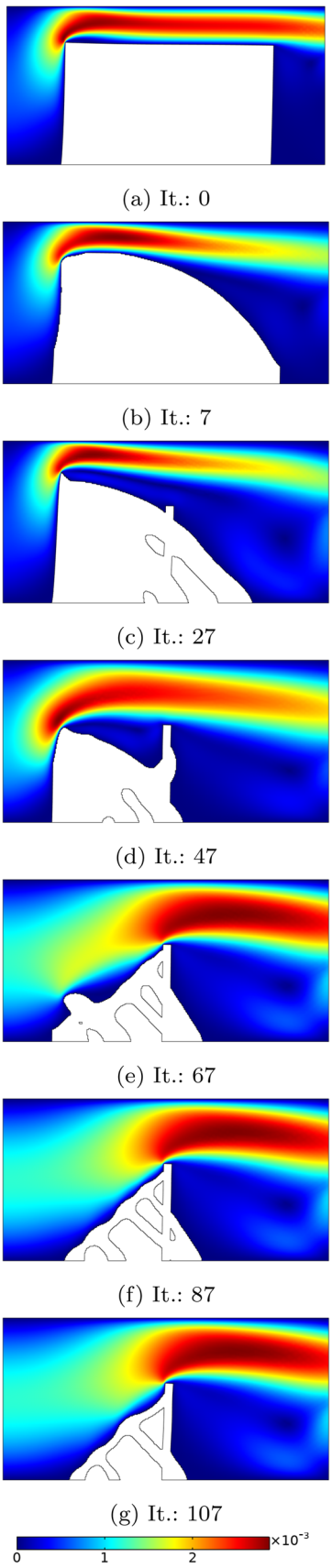

Fig. 12 Velocity field (in m/s) of the snapshots during the optimization for $p = 5$ ▶

grid has 44,800 elements (280×160 grid points) distributed only in the structural design domain. Mesh refinement is not directly linked to optimization grid size. Therefore, the increase of points in the optimization grid in order to obtain topologies with higher resolution does not lead to a higher computational cost, as the finite element mesh can be kept in a computationally convenient size. The possibility of using coarse meshes in contrast to the higher grid resolution is one of the possible advantages of the TOBS-GT approach. On the other hand, the consideration of a dense FE mesh and a coarse optimization grid should tend to produce smoother fields and, therefore, similar results but with a higher computational cost. The use of coarser meshes reduces the overall time and challenges of the FSI computation, since the bottleneck of the optimization is the finite element analysis. While the FEA solver can take between 20 and 70 seconds each iteration, the ILP problem takes less than 1 second to be computed (see Fig. 15). In addition, the geometry trimming procedure takes on average less than 1 second to be executed as well as the generation of a new FEA mesh at every iteration. Therefore, both processes are significantly cheap compared to the FEA forward problem. Thus, the TOBS-GT method promises to be relatively cheap for optimizing problems with a high degree of physical complexity.

5.3 The billboard—3D "wet" optimization

This example solves the "wet" optimization case of a flexible three-dimensional billboard-like structure immersed in a fluid flow channel of dimension $10 \times 6 \times 6$ mm. The problem illustration is shown in Fig. 16. A 0.1 mm thick plate is suspended by a circular main column with a diameter of 0.33 mm, located on the bottom boundary of the fluid channel and centered on the z–direction , with a distance of 3.0 mm from the inlet Γ_{in}. The objective of this example is to design a support structure behind the suspended plate. The design domain Ω_{s} is located behind the structure and is connected to the main column at a height of 2.0 mm, and has a dimension of $3 \times 2 \times 0.5$ mm. The solid material properties for this example is chosen to have Young's modulus $E_0 = 4 \times 10^3$ Pa and Poisson's ratio $\nu = 0.3$. Fluid is considered to be air (density $\rho_{\text{f}} = 1.27\,\text{kg/m}^3$ and dynamic viscosity $\mu_{\text{f}} = 1.72 \times 10^{-5}\,\text{Pa s}$). Maximum inlet velocity v_{in} is defined to 0.01 m/s.

A parabolic fluid flow enters the channel Γ_{in} with velocity $\mathbf{v} = v_{\text{in}}(y/H)^{\frac{1}{7}}$, where H corresponds to the height of the three-dimensional flow channel—in this case 6.0 mm—and y is the vertical coordinate for each input point. A pressure condition $p_{\text{out}} = 0$ is established at the outflow Γ_{out}. The following conditions are imposed on the walls of the fluid channel:

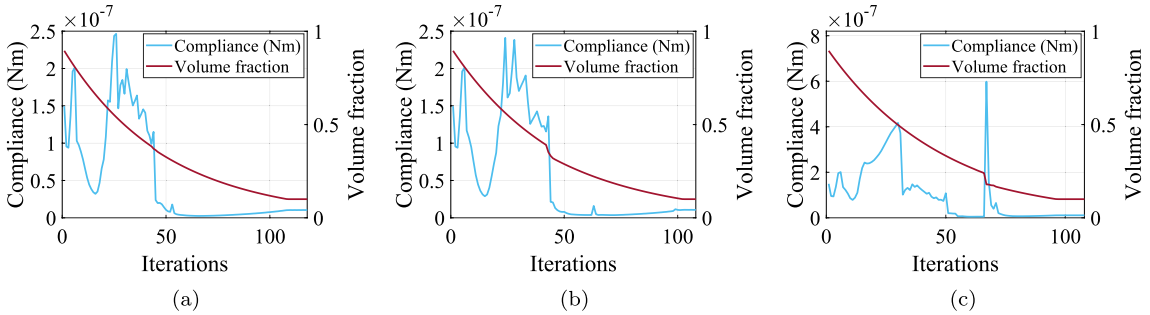

Fig. 13 Evolution history of the objective function (mean compliance) and constraint function (volume) for the cases: **a** $p = 3$, **b** $p = 5$ and **c** $p = 10$

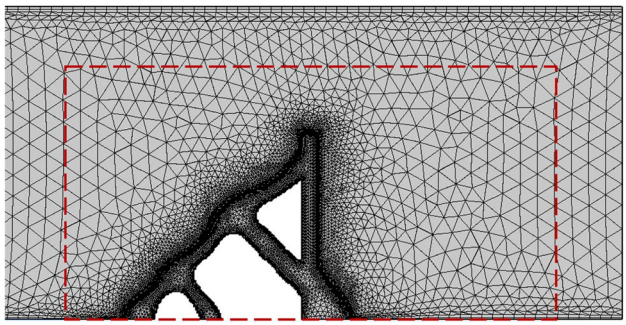

Fig. 14 Finite element mesh—14,637 triangular and 560 quadrilateral elements—for the final optimized design ($p = 5$). The red dashed line represents the initial design domain

lateral and upper boundaries Γ_{sw} are set to slip condition, lower boundary Γ_w and the fluid–structure interface Γ_{fs} are set to non-slip condition. The displacements in the bottom structural boundary of the main column Γ_u are fixed, i.e., $\mathbf{u} = 0$. The TOBS-GT method is considered to minimize the mean compliance of structural support subject to a volume fraction constraint of $\bar{V} = 30\%$. An optimization grid of size $16 \times 80 \times 120$ is applied and it is located on the back of the board corresponding to the gray region (see Fig. 16). The penalty factor adopted for the material model is $p = 5$. A filter radius of 2 grid sizes is considered. The optimization parameters used are $\epsilon = 0.02$ and $\beta = 0.05$. Some views of the optimized structural design are shown in Fig. 17. The optimized support is connected to the main column of the structure with a greater amount of solid materials being deposited in this region. However, it is still possible to observe the occurrence of large displacements as shown in Fig. 18. The TOBS-GT optimization grid can be placed anywhere of interest in the structure, as in this example where the grid points are considered to be at a height on the y-axis. In this way, any structural component can be optimized using the TOBS-GT approach, as long as the optimization grid $\{0, 1\}$ is placed accordingly. In addition, when considering large displacements, it is important to identify the frame of reference where the points are evaluated. Figure 18

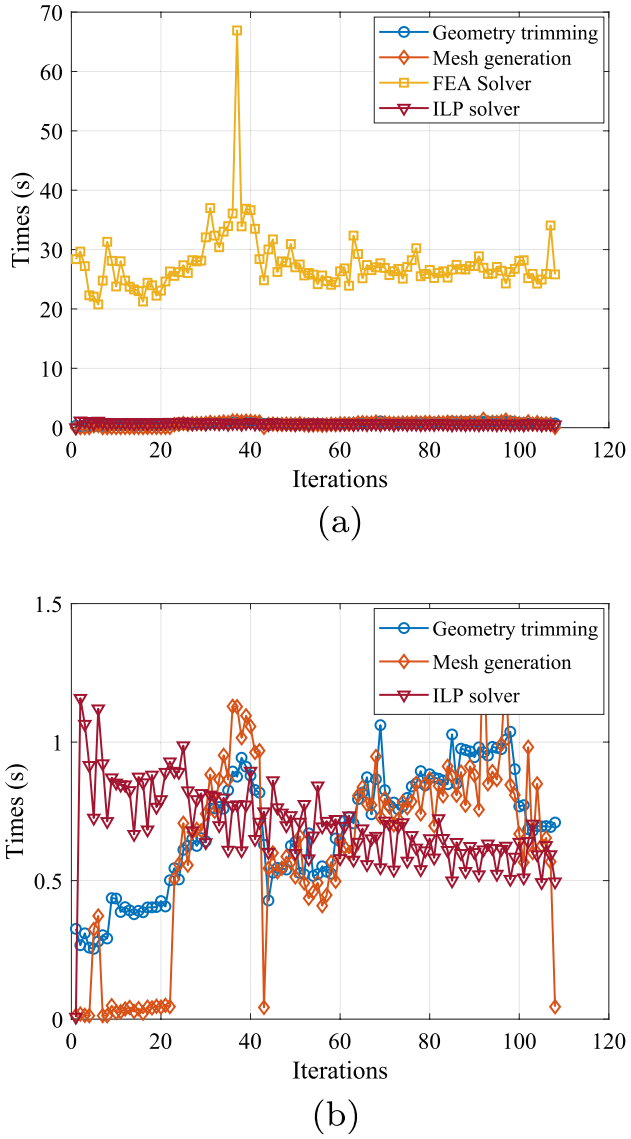

Fig. 15 Breakdown computation times of each iteration for the case with $p = 5$ using the TOBS-GT method: **a** for the main optimization steps **b** omitting the FEA solver times

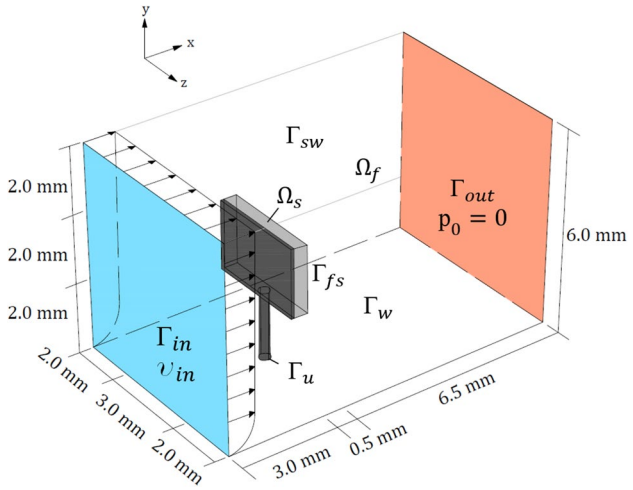

Fig. 16 The 3D billboard problem

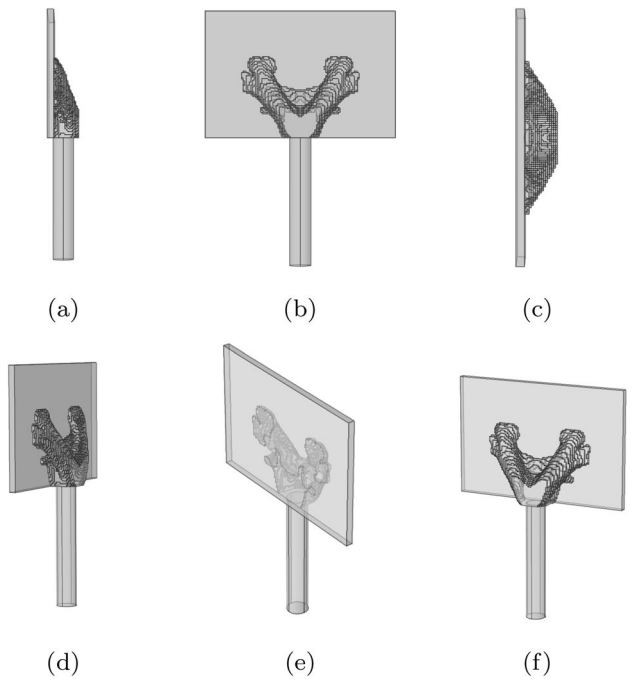

Fig. 17 Optimized structural support for 3D FSI problem including large displacements: **a** side view, **b** back view, **c** top view and **d**–**f** angled views

presents the streamlines of the velocity profile for optimized structural support and the zoomed structure in a multislice velocity field plot.

6 Conclusions

A spatial-material framework is employed to extend the TOBS-GT method (Picelli et al. 2020a) for optimizing FSI problems including large displacements. The optimized design of structures under viscous fluid loads is achieved through a decoupled analysis, where the optimization grid and the physical analysis are used as independent modules. This approach shows to be convenient when modelling two different physics, such as in the present FSI problem. A decrease in the total number of finite elements used is achieved if compared to the fixed optimization grid size. Thus, the optimization of the FSI topology is performed with a reasonably lower computational cost. The approach, named the TOBS-GT method, integrates the standard TOBS solver Sivapuram and Picelli (2018) with an external finite element analysis package. For considering large structural displacements, the FSI system is computed in the spatial (Eulerian) and material (Langragian) frame which allows the identification and tracking of the deformed FSI interface. The solid domain is solved using an elastic formulation with geometrical nonlinearities. The cases of "dry" and "wet" optimization are solved. Different solutions are obtained when comparing small and large displacements studies. The extension of the proposed methodology to 3D structures is direct. The inclusion of material nonlinearity, wall smoothing for high Reynolds numbers and the extension of the present methodology to non-FSI problems—such as single physics problems and multi-material problems—are possible directions for future research.

Appendix

This appendix presents the analysis by finite differences used to verify the sensitivities from Eq. 28 obtained via semi-automatic differentiation. The model analyzed is a variation of the wall problem and is shown in Fig. 19a. A viscous fluid flow enters through the micro-channel inlet with $Re = 10$, with a parabolic velocity profile. At the outlet channel a pressure condition $p = 0$ is imposed. Non-slip conditions are applied to the walls of the fluid channel. The solid structure is fixed at its bottom, therefore displacements in this face are prescribed as zero ($\mathbf{u} = 0$). The sensitivities described by Eq. 28 are computed in nine points within the design domain Ω_s, being six of them at the fluid–structure boundaries. The fluid is considered to be water, i.e., with density $\rho = 1000$ kg/m^3 and dynamic viscosity $\mu = 0.001$ Pa s, and the solid material is chosen to have Young's modulus $E = 2.4 \times 10^5$ Pa and Poisson's ratio $\nu = 0.3$. Sensitivities are calculated by

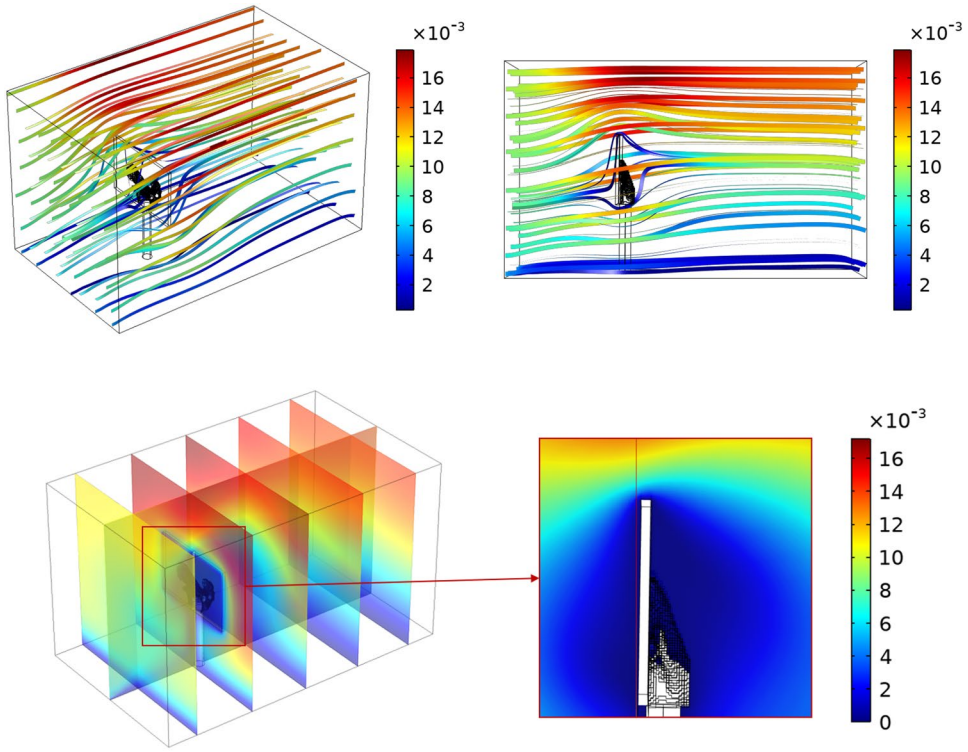

Fig. 18 Fluid velocity field (in m/s) around optimized 3D structure via TOBS-GT method

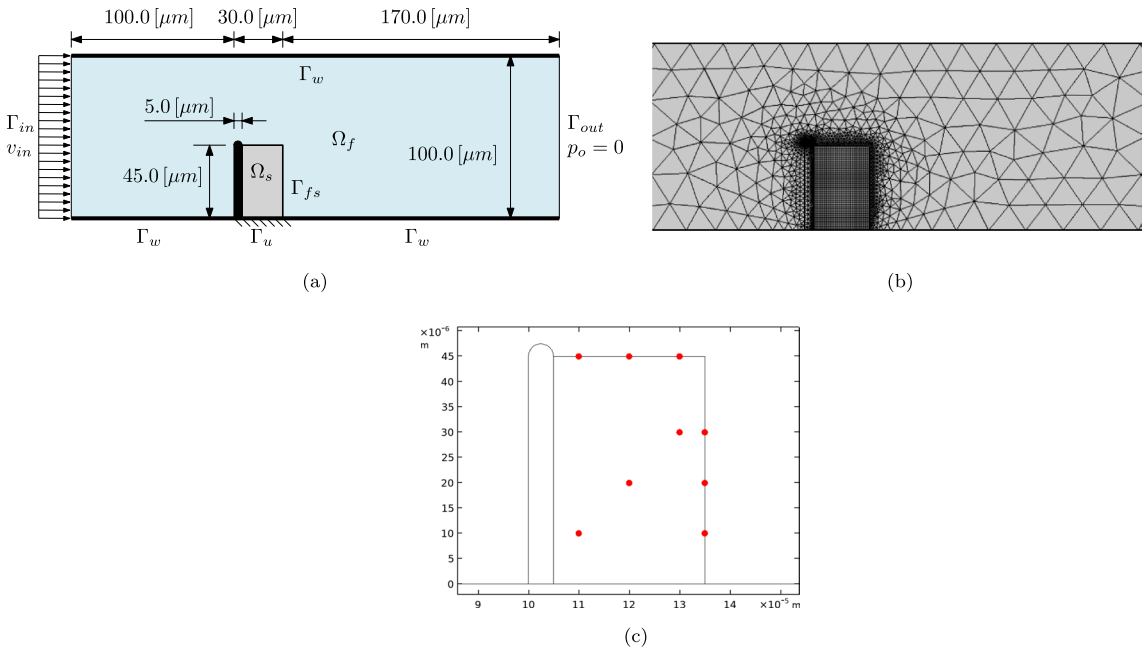

Fig. 19 Model used to carry out finite differences analysis: **a** illustration of the model, **b** finite element mesh and **c** points in the design domain

semi-automatic differentiation and then checked by the finite differences method. For the finite difference analysis, the step 1×10^{-5} is considered. Figure 19a and c present, respectively, the considered points in finite differences analysis and the finite element mesh used. The finite element mesh employed and the evaluated points are shown in Fig. 19b. Figure 20a presents the velocity field for this model and Fig. 20b plots of the structure including large

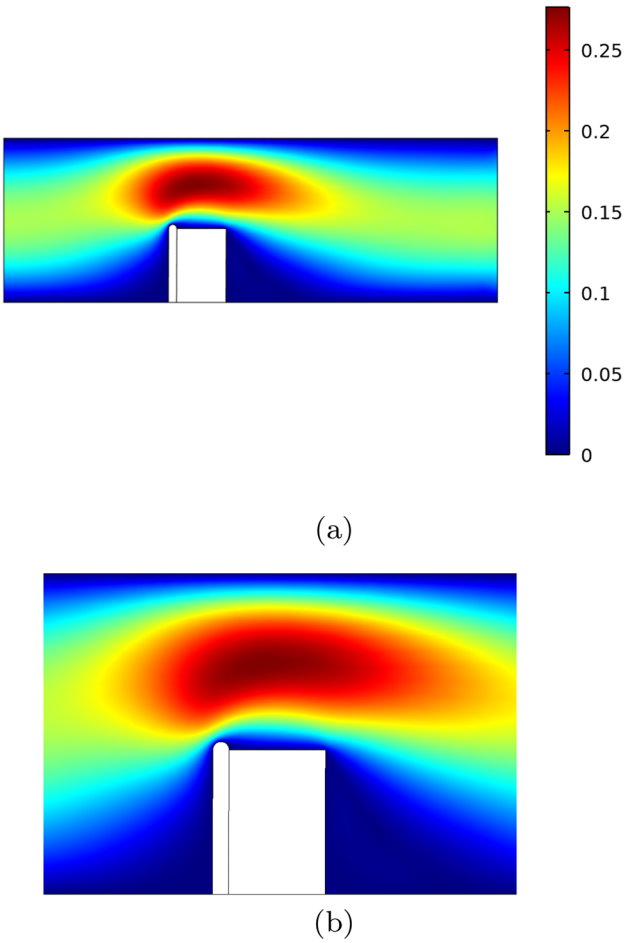

Fig. 20 Fluid velocity field (m/s) of the model considered in the finite differences analysis with $Re = 10$: **a** plot of the velocity field of the problem and **b** zoomed image

displacements with zoomed. Table 2 shows the sensitivity values obtained via semi-automatic symbolic differentiation and via finite differences. The maximum relative difference between the two methods does not exceed 1%, which is considerably small and validates the usability of the semi-automatic differentiation tool available in the software.

Acknowledgements The first author thanks FAPESP (São Paulo Research Foundation), grant 2019/26809-7, and the last author thanks the Young Investigators Awards program by FAPESP, grants 2018/05797-8 and 2019/01685-3. The fifth author thanks the financial support of CNPq (Brazilian National Council for Research and Development) under grant 302658/2018-1 and FAPESP under grant 2013/24434-0. The third, fourth, fifth and sixth authors also acknowledge the support from the RCG2I (Research Centre for Greenhouse Gas Innovation), hosted by the University of São Paulo (USP) and sponsored by FAPESP (2014/50279-4 and 2020/15230-5) and Shell Brazil.

Declarations

Conflict of interest The authors declare that they have no conflict of interest.

Replication of results The results presented in this work can be reproduced by following the algorithms and formulations presented in detail herein. The TOBS implementation is presented in www.github.com/renatopicelli/tobs and in Picelli et al. (2020b).

References

Andreasen CS, Sigmund O (2013) Topology optimization of fluid-structure interaction problems in poroelasticity. Comput Methods Appl Mech Eng 258:55–62

Bazilevs Y, Takizawa K, Tezduyar T (2013) Computational fluid-structure interaction: methods and applications. Wiley series in computational mechanics, Wiley, Chichester

Bendsøe MP, Sigmund O (2003) Topology optimization - theory, methods and applications. Springer, Berlin

Bodnár T, Galdi G, Nečasová (2014) Fluid-structure interaction and biomedical applications

Bungartz HJ, Schäfer M (2006) Fluid-structure interaction: modelling, simulation. Optimization, Berlin

Casadei F, Halleux J, Sala A, Chillè F (2001) Transient fluid–structure interaction algorithms for large industrial applications. Computer Methods in Applied Mechanics and Engineering 190(24):3081–3110, advances in Computational Methods for Fluid-Structure Interaction

Feppon F, Allaire G, Dapogny C, Jolivet P (2020) Topology optimization of thermal fluid-structure systems using body-fitted meshes and parallel computing. J Comput Phys 417(109):574

Table 2 Finite differences analysis results; AD = automatic differentiated sensitivities; FD = sensitivities obtained by finite differences

Point	Coordinates (x, y) (μm)	AD (kNm)	FD (kNm)	Difference (%)
1	(11.0, 10.0)	-0.7416×10^{-13}	-0.7430×10^{-13}	0.1875
2	(12.0, 20.0)	-0.3907×10^{-13}	-0.3905×10^{-13}	0.0480
3	(13.0, 30.0)	-0.1397×10^{-13}	-0.1391×10^{-13}	0.3796
4	(13.5, 10.0)	-0.6738×10^{-13}	-0.6724×10^{-13}	0.2180
5	(13.5, 20.0)	-0.2530×10^{-13}	-0.2520×10^{-13}	0.3900
6	(13.5, 30.0)	-0.0623×10^{-13}	-0.0616×10^{-13}	0.9927
7	(11.0, 45.0)	-0.1360×10^{-13}	-0.1663×10^{-13}	0.2250
8	(12.0, 45.0)	-0.0084×10^{-13}	-0.0085×10^{-13}	0.8108
9	(13.0, 45.0)	-0.0261×10^{-13}	-0.0260×10^{-13}	0.4803

Galdi G, Rannacher R (2010) Fundamental Trends in Fluid-structure Interaction. Contemporary challenges in mathematical fluid dynamics and its applications, World Scientific, Singapore

Gatzhammer B (2014) Efficient and flexible partitioned simulation of fluid-structure interactions. PhD thesis, Technical University of Munich, Germany

Gresho PM, Sani RL (2000) Incompressible Flow and the Finite Element Method. Wiley

Haftka RT, Gürdal Z (1991) Elements of structural optimization, 3rd edn. Kluwer Academic Publishers, Amsterdam

Hami A, Radi B (2017) Fluid-structure interactions and uncertainties: Ansys and fluent tools. Reliability of multiphysical systems, Wiley, mechanical engineering and solid mechanics

Huang X, Xie YM (2007) Convergent and mesh-independent solutions for the bi-directional evolutionary structural optimization method. Finite Elem Anal Des 43:1039–1049

Jenkins N, Maute K (2015) Level set topology optimization of stationary fluid-structure interaction problems. Struct Multidisc Optim 52(1):179–195

Jenkins N, Maute K (2016) An immersed boundary approach for shape and topology optimization of stationary fluid-structure interaction problems. Struct Multidisc Optim 54:1191–1208

Kamakoti R, Shyy W (2004) Fluid-structure interaction for aeroelastic applications. Prog Aerosp Sci 40(8):535–558

Kook J, Jensen JS (2017) Topology optimization of periodic microstructures for enhanced loss factor using acoustic-structure interaction. Int J Solids Struct 122–123:59–68

Land AH, Doig AG (1960) An automatic method of solving discrete programming problems. Econometrica 28:497–520

Li H, Kondoh T, Jolivet P, Furuta K, Yamada T, Zhu B, Izui K, Nishiwaki S (2021) Three-dimensional topology optimization of a fluid-structure system using body-fitted mesh adaption based on the level-set method. Appl Math Model 101:276–308

Lund E, Møller H, Jakobsen L (2003) Shape design optimisation of stationary fluid-structure interaction problems with large displacement and turbulence. Struct Multidisc Optim 25:383–392

Lundgaard C, Alexandersen J, Zhou M, Andreasen C, Sigmund O (2018) Revisiting density-based topology optimization for fluid-structure-interaction problems. Struct Multidisc Optim 58:969–995

Maute K, Allen M (2004) Conceptual design of aeroelastic structures by topology optimization. Struct Multidisc Optim 27(1–2):27–42

Païdoussis MP (1998) Fluid-structure interactions: slender structures and axial flow, vol 1. Academic Press

Picelli R, Vicente WM, Pavanello R (2015) Bi-directional evolutionary structural optimization for design-dependent fluid pressure loading problems. Eng Optim 47(10):1324–1342

Picelli R, Vicente WM, Pavanello R (2017) Evolutionary topology optimization for structural compliance minimization considering design-dependent FSI loads. Finite Elem Anal Des 135:44–55

Picelli R, Neofytou A, Kim HA (2019) Topology optimization for design-dependent hydrostatic pressure loading via the level-set method. Struct Multidisc Optim 60:1313–1326

Picelli R, Ranjbarzadeh S, Sivapuram R, Gioria RS, Silva ECN (2020a) Topology optimization of binary structures under design-dependent fluid-structure interaction loads. Struct Multidisc Optim 62:2101–2116

Picelli R, Sivapuram R, Xie YM (2020b) A 101-line MATLAB code for topology optimization using binary variables and integer programming. Struct Multidisc Optim 63:935–954

Picelli R, Moscatelli E, Yamabe P, Alonso D, Ranjbarzadeh S, Gioria R, Meneghini J, Silva E (2022) Topology optimization of turbulent fluid flow via the TOBS method and a geometry trimming procedure. Struct Multidisc Optim 65:1–25

Richter T (2017) Fluid-structure Interactions: models, analysis and finite elements. Lecture notes in computational science and engineering, Springer, New York

Sivapuram R, Picelli R (2018) Topology optimization of binary structures using integer linear programming. Finite Elem Anal Des 139:49–61

Sivapuram R, Picelli R (2020) Topology design of binary structures subjected to design-dependent thermal expansion and fluid pressure loads. Struct Multidisc Optim 61:1877–1895

Vicente WM, Picelli R, Pavanello R, Xie YM (2015) Topology optimization of frequency responses of fluid-structure interaction systems. Finite Elem Anal Des 98:1–13

Wriggers P (2008) Nonlinear finite element methods. Springer, Berlin

Yoon GH (2010) Topology optimization for stationary fluid-structure interaction problems using a new monolithic formulation. Int J Numer Meth Eng 82:591–616

Yoon GH (2014) Stress-based topology optimization method for steady-state fluid-structure interaction problems. Comput Methods Appl Mech Eng 278:499–523

Zhu J, Zhou H, Wang C, Zhou L, Yuan S, Zhang W (2021) A review of topology optimization for additive manufacturing: status and challenges. Chin J Aeronaut 34(1):91–110